On Antilock Braking Systems With Road Preview Through Nonlinear Model Predictive Control

Gaetano Tavolo, Kai Man So, Davide Tavernini, Pietro Perlo, and Aldo Sorniotti, *Member, IEEE*

***Abstract*—State-of-the-art antilock braking systems (ABS) are reactive, i.e., they activate after detecting that wheels tend to lock in braking. With vehicle-to-everything (V2X) connectivity becoming a reality, it will be possible to gather information on the tire–road friction conditions ahead, and use these data to enhance wheel slip control performance, especially during abrupt friction level variations. This study presents a nonlinear model predictive controller (NMPC) for ABS with preview of the tire–road friction profile. The potential benefits, optimal prediction horizon, and robustness of the preview algorithm are evaluated for different dynamic characteristics of the brake actuation system, through an experimentally validated simulation model. Proof-of-concept experiments with an electric vehicle prototype highlight the real-time capability of the proposed NMPC ABS, and the associated wheel slip control performance improvements in braking maneuvers with high-to-low friction transitions.**

***Index Terms*—Antilock braking system (ABS), connectivity, nonlinear model predictive control (NMPC), preview, tire–road friction, vehicle-to-everything (V2X), wheel slip control.**

I. Introduction

AUTOMOTIVE antilock braking systems (ABS) prevent wheel locking during braking, by maintaining or reducing the braking torque, thus ensuring vehicle steerability. ABS technology is well-known and rather mature. The first modulating brake force regulator patent dates back to 1928 [1]. ABS implementations were initially used in the aviation and railway industries in the 1950s, before expanding to the automotive sector in the 1970s. ABS has become mandatory for all new passenger cars in the European Union since 2004, and in the United States since 2012.

Today's production automotive ABS strategies are heuristic rule-based feedback controllers [2]. They reduce or maintain the brake torque when the wheel slip and/or wheel decelerations reach critical levels. Moreover, because of the conventional hydraulic arrangement of ABS units, which does not permit continuous feedback pressure control, production ABS algorithms tend to prescribe discrete levels of pressure variation rate, which limit performance. With the advent of brake-by-wire systems and advanced hydraulic brake modulation units enabling accurate and swift braking torque control [3], the literature has transitioned toward ABS algorithms based on continuous pressure or torque modulation, e.g., through proportional integral derivative (PID) controllers, linear quadratic regulators, classical robust controllers, sliding mode controllers (SMCs), and model predictive controllers (MPCs). All previous techniques are mentioned and contrasted in the recent survey paper [4]. SMC and MPC are particularly promising control structures for wheel slip control. More specifically, with respect to (w.r.t.) SMC, Phadke et al. [5] discuss a disturbance observer within a sliding mode scheme characterized by a novel nonlinear sliding surface formulation to improve the slip ratio tracking performance. Similarly, Choi et al. [6] deal with SMC chattering, which is the main demerit of SMC implementations, through an estimation of the unknown disturbances. Both schemes in [5] and [6] provide desirable robustness characteristics, which is the typical benefit of SMC techniques, together with the lack of need for detailed model parameters. For MPC, the review in [4] concludes that it is a promising approach "in terms of performance and robustness" compared to the other considered algorithms, and that it "should be further investigated […] to understand its full capabilities."

A significant body of research has dealt with MPCs for ABS, which include an optimization process considering the prediction of the system dynamics along a finite time horizon while embedding constraints. For example, the simulation results in [4] highlight the superiority of a nonlinear MPC (NMPC) ABS over a rule-based ABS, with quicker response times, less underbraking, and improved comfort due to the smoother control. In [7], a linear MPC is simulated on an electric vehicle (EV) with in-wheel machines. Only the motor torque is modulated during the ABS events, because of the faster dynamics of the electric powertrains w.r.t. the friction brakes. Linear and nonlinear

Manuscript received 27 March 2023; revised 30 June 2023 and 25 August 2023; accepted 4 September 2023. This work was supported by the Horizon 2020 Programme of the European Commission under Grant 101006953 (Multi-Moby project). *(Corresponding author: Aldo Sorniotti.)*

Gaetano Tavolo is with the Centre for Automotive Engineering, University of Surrey, GU2 7XH Guildford, U.K., and also with the Interactive Fully Electrical VehicleS, 10040 Turin, Italy (e-mail: g.tavolo@surrey.ac.uk).

Kai Man So and Davide Tavernini are with the Centre for Automotive Engineering, University of Surrey, GU2 7XH Guildford, U.K. (e-mail: k.so@surrey.ac.uk; d.tavernini@surrey.ac.uk).

Pietro Perlo is with the Interactive Fully Electrical VehicleS, 10040 Turin, Italy (e-mail: pietro.perlo@ifevs.com).

Aldo Sorniotti is with the Department of Mechanical and Aerospace Engineering, Politecnico di Torino, 10129 Torino, Italy, and also with the Centre for Automotive Engineering, University of Surrey, GU2 7XH Guildford, U.K. (e-mail: aldo.sorniotti@polito.it).

Color versions of one or more figures in this article are available at https://doi.org/10.1109/TIE.2023.3314917.

Digital Object Identifier 10.1109/TIE.2023.3314917

MPCs for ABS are simulated and assessed in [8], with a focus on the blending between the friction and regenerative braking contributions, where the linear controller performs worse at low vehicle speeds. Ma et al. [9] simulate NMPC algorithms for traction control and ABS for EVs, and considers the effect of road surface unevenness. In [10], an NMPC ABS, including a simplified thermal tire model, is assessed in simulation, performing better throughout a wide range of environmental conditions than the corresponding algorithm neglecting tire temperature effects. The NMPC ABS in [11] embeds a fractional extremum seeking algorithm to establish the optimal slip ratio without knowledge of the tire–road friction coefficient. The simulations show improved search speed, compared to the more conventional integer order extremum seeking method.

A drawback of MPC implementations for wheel slip control is represented by the computational requirements for real-time implementation. To alleviate computational load, Gaurkar et al. [12] formulate the optimal control problem of an NMPC ABS to be convex. An explicit NMPC ABS approach is proposed in [13], in which the solution of the optimal control problem is computed offline, and stored in the flash memory of the considered real-time platform. The controller achieves shorter stopping distance and better reference slip tracking than a benchmarking PID controller.

With the advent of modern control units and efficient solvers, real-time implicit (i.e., computing the solution online) MPCs for automotive applications at low time step are now feasible, e.g., see the experimentally tested MPC ABS for EVs in [14], providing shorter braking distance and better comfort on wet surfaces than an SMC. In [15], a linear MPC ABS, including friction and regenerative brake blending, is tested in simulations and experiments on an in-wheel motor EV, with comparisons to an architecture combining a static brake blending allocation, and a proportional integral (PI) ABS algorithm. In [16], [17], [18], and [19], NMPCs using the qpOASES solver of the ACADO toolkit [20] are experimentally demonstrated with various EVs. The algorithms in [16], [17], and [18] receive the tire–road friction data through vehicle-to-everything (V2X), for pre-emptive traction and/or anti-jerk control. Guastadisegni et al. [19] experimentally demonstrate an NMPC for pre-emptive braking, which slows down the vehicle if its speed is too high w.r.t. the upcoming road curvature and friction conditions.

With respect to the onboard methods for estimating tire–road friction conditions, multiple techniques have been proposed, e.g., using Kalman [21] and particle filters [22] based on inertial measurement units and other typical vehicle dynamics sensors, as well as more innovative methods based on optical sensors [23], cameras [23], [24], or radars [25]. In parallel, next-generation connected vehicles and V2X [26] could pre-emptively identify hazardous road conditions through cooperative friction estimation. In fact, the tire–road friction information could be sent to the cloud via V2X, and a map of the low tire–road friction patches ahead would be generated and transmitted to upcoming vehicles. Volvo Cars has trialed a similar system [27], which passively and pre-emptively notifies human drivers about icy road spots. However, there is a current lack of studies on active ABS implementations with tire–road friction preview and their potential benefits.

To address the identified gap, the research of this work provides the following contributions:

1) NMPC algorithms (see Section II) using the friction information ahead for pre-emptive ABS control. NMPC is the natural choice for this application, as it accounts for system nonlinearities, and can incorporate the upcoming friction coefficient profile.
2) Simulation studies (see Section IV) via an experimentally validated model to analyze: first, the relationship between the brake hardware actuation dynamics and the required prediction horizon (H_P) for good wheel slip performance with tire–road friction preview; and second, the robustness of the NMPCs to uncertainties, disturbances, and errors in the V2X data.
3) Proof-of-concept experimental assessment of the real-time capability and performance of the NMPCs with and without road preview, including the comparison with a benchmarking pre-emptive PID controller. The algorithms are demonstrated on an EV prototype with hydraulically actuated brakes (HABs) (see Section V).

II. Controller Design

A. Considered Controllers

Four NMPC ABS algorithms have been developed in this research, which are as follows:

1) A pre-emptive NMPC with preview of the upcoming tire–road friction level, and considering the actuation dynamics of the brake hardware in the prediction model. This is referred to as "Pre-NMPC with τ_{hb}" in the remainder.
2) The same as above, but without consideration of the actuation dynamics ("Pre-NMPC w/o τ_{hb}").
3) A benchmarking NMPC without tire–road friction preview, but considering the brake actuation dynamics ("NMPC with τ_{hb}").
4) The same as "NMPC with τ_{hb}", but excluding consideration of the actuation dynamics ("NMPC w/o τ_{hb}").

B. Control System Architecture

Fig. 1 is a simplified schematic of the pre-emptive NMPC architecture, where the subscript $i = F, R$ indicates the front or rear axles, and $j = L,\ R$ indicates the left or right wheels. The high-level controller, i.e., the NMPC ABS, receives the tandem master cylinder (TMC) pressure P_{TMC} measured by a sensor, and—if necessary—reduces it to a reference modified brake caliper pressure level $P_{b,ij,mod}$ to ensure desirable wheel slip dynamics. The external inputs to the high-level controller include the longitudinal vehicle speed (V_x), longitudinal acceleration (a_x), angular wheel speed (ω_{ij}), and actual caliper pressure ($P_{b,ij}$). Moreover, the ABS implementations with road preview receive: first, the vector ($\boldsymbol{\mu_{ij,fut}}$) of the upcoming tire–road friction factor values along the N steps of the prediction horizon H_P, i.e., $\boldsymbol{\mu_{ij,fut}} = [\mu_{ij,fut,0}, \mu_{ij,fut,1}, .., \mu_{ij,fut,N}]$ (here and

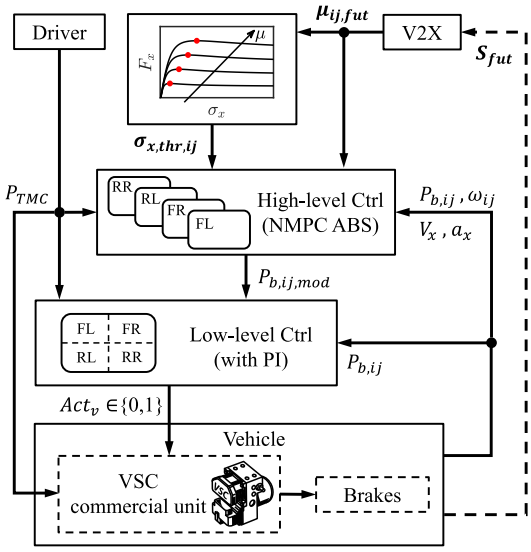

Fig. 1. Simplified schematic of the ABS control structure.

in the remainder, bold fonts are used to indicate vectors); and second, the corresponding vector ($\boldsymbol{\sigma_{x,thr,ij}}$) of slip ratio thresholds, which are based on predetermined force-slip lookup tables for each tire. On the contrary, the non-pre-emptive controllers only use the present tire–road friction factors and corresponding slip threshold values, which are maintained constant along H_P.

The centralized low-level controller actuates the relevant valves of the vehicle stability control (VSC) unit to track $P_{b,ij,mod}$ by using $P_{b,ij}$ as feedback. The discrete (off/on) actuation signals are indicated with Act_v, where the subscript v refers to a generic valve or the motor pump (see Section III).

C. Internal Model

The internal model of "Pre-NMPC with τ_{hb}" is expressed through the following continuous time formulation:

$$\dot{\boldsymbol{x}}(t) = f(\boldsymbol{x}(t), \boldsymbol{u}(t)) \tag{1}$$

where the state vector $\boldsymbol{x}$ is:

$$\boldsymbol{x} = [\omega_{FL}, \omega_{FR}, \omega_{RL}, \omega_{RR}, T_{b,FL}, T_{b,FR}, T_{b,RL}, T_{b,RR}] \tag{2}$$

with $T_{b,ij}$ being the friction braking torques. The control action is defined as:

$$\boldsymbol{u} = [\Delta T_{b,FL}, \Delta T_{b,FR}, \Delta T_{b,RL}, \Delta T_{b,RR}, \varepsilon_{\sigma_{x,FL}}, \varepsilon_{\sigma_{x,FR}}, \varepsilon_{\sigma_{x,RL}}, \varepsilon_{\sigma_{x,RR}}] \tag{3}$$

where $\Delta T_{b,ij}$ is the braking torque regulation (which is negative during ABS interventions, see (20)); and $\varepsilon_{\sigma_{x,ij}}$ is the slack variable of the longitudinal tire slip ratio, which allows the implementation of a soft constraint on the slip ratio error (explained later in (20)).

The first equation of the internal model of each corner is the wheel moment balance:

$$\dot{\omega}_{ij} = \frac{-T_{b,ij} - F_{x,ij} R_{w,i}}{J_{\omega,i}} \tag{4}$$

where $J_{\omega,i}$ is the wheel mass moment of inertia; $R_{w,i}$ is the wheel radius; and $F_{x,ij}$ is the longitudinal tire force, which is computed through a simplified version of the Pacejka magic formula (MF) [28]:

$$F_{x,ij} = \mu_{x,ij} F_{z,ij} \tag{5}$$

where $F_{z,ij}$ is the vertical tire load, considered constant along H_P; and $\mu_{x,ij}$ is the longitudinal tire force coefficient:

$$\mu_{x,ij} = D_{ij} \sin\left(C_{0,i} \tan^{-1}\left(B_{ij}\sigma_{x,ij}\right)\right) \tag{6}$$

with $\sigma_{x,ij}$ being the longitudinal tire slip ratio:

$$\sigma_{x,ij} = \frac{\omega_{ij} R_{w,i} - V_x}{V_x} \tag{7}$$

B_{ij} and D_{ij} are the MF parameters:

$$B_{ij} = B_{0,i} / \mu_{ij,fut} \tag{8}$$

$$D_{ij} = D_{0,i}\, \mu_{ij,fut} \tag{9}$$

which have been scaled based on the tire–road friction factor $\mu_{ij,fut}$ obtained from V2X. $B_{0,i}$, $C_{0,i}$, and $D_{0,i}$ are the nominal MF tire parameters for high-friction conditions. Given the short H_P values of this application, V_x is considered constant along the prediction.

The vertical tire load in (5) is approximated as:

$$F_{z,F/Rj} = \frac{1}{2} \frac{m}{l_F + l_R} \left[g l_{R/F} \mp H_{CG} a_x\right] \tag{10}$$

where m is the total EV mass; g is the gravitational acceleration; H_{CG} is the center of gravity height; and l_F and l_R are the front and rear semi-wheelbases, respectively.

The second equation of the internal model of the corner approximates the nonlinear brake actuation dynamics as a first-order system:

$$\dot{T}_{b,ij} = \frac{T_{b,drv,i} + \Delta T_{b,ij} - T_{b,ij}}{\tau_{hb}} \tag{11}$$

where τ_{hb} is the time constant of the HAB system; and $T_{b,drv,i}$ is the driver braking torque demand (always positive) for a single wheel, calculated as:

$$T_{b,drv,i} = P_{TMC}\, A_{wc,i} F_{brk,i} R_{disc,i} \tag{12}$$

with $A_{wc,i}$ being the area of wheel cylinder of the brake caliper; $F_{brk,i}$ being the respective brake factor, defined as twice the friction coefficient between the brake pads and disc ($\mu_{pad,i}$); and $R_{disc,i}$ being the effective disc radius. Equations (4)–(12) are repeated for each corner ij.

The pre-emptive capability of the controller stems from the V2X-obtained $\boldsymbol{\mu_{ij,fut}}(k)$ at the current time step k being a vector. $\boldsymbol{\mu_{ij,fut}}(k)$ is computed from the $\boldsymbol{S_{fut}}(k)$ vector, which includes the predicted traveled distance values:

$$\boldsymbol{\mu_{ij,fut}}(k) = f_{\mu_{ij,fut}}\left[\boldsymbol{S_{fut}}(k)\right] \tag{13}$$

where $f_{\mu_{ij,fut}}$ is set as a map in this study. $\boldsymbol{S_{fut}}(k)$ is generated under the assumption of constant speed $V(k)$ along H_P:

$$\boldsymbol{S_{fut}}(k) = S(k)\,\mathbf{1} + V(k)\left[\boldsymbol{t_{fut}} - t_{fut,0}\mathbf{1}\right] \tag{14}$$

with $S(k)$ being the current vehicle position; $\mathbf{1}$ an all-ones vector with $N+1$ dimension; $\boldsymbol{t_{fut}} = [t_{fut,0}, t_{fut,1}, .., t_{fut,N}]$ the future time value vector with $N+1$ points equally spaced by a constant time step T_s; and $t_{fut,0} = t(k)$ the current time instant. For the non-pre-emptive implementations "NMPC with τ_{hb}" and "NMPC w/o τ_{hb}", $\boldsymbol{\mu_{ij,fut}}$ consists of identical components, equal to the current tire–road friction factor.

The internal model for the controllers without consideration of actuation dynamics differs in the state vector, as the angular wheel speeds are the only states:

$$\boldsymbol{x} = [\omega_{FL}, \omega_{FR}, \omega_{RL}, \omega_{RR}] \tag{15}$$

Equation (11) is omitted from the model, and thus (4) is replaced with:

$$\dot{\omega}_{ij} = \frac{-T_{b,drv,i} - \Delta T_{b,ij} - F_{x,ij} R_{w,i}}{J_{\omega,i}} \tag{16}$$

When the high-level controller is activated, i.e., $\Delta T_{b,ij} < 0$, the torque control actions are converted—outside the NMPC—into reference pressures for the low-level controller (see Fig. 1):

$$P_{b,ij,mod} = \frac{T_{b,drv,i} + \Delta T_{b,ij}}{A_{wc,i} F_{brk,i} R_{disc,i}} \tag{17}$$

D. Nonlinear Optimal Control Problem

The nonlinear optimal control problem can be defined as the minimization of the cost function J in discrete time form:

$$\min_{\boldsymbol{u}} J\left(\boldsymbol{x}\left(0\right), \boldsymbol{u}\left(\cdot\right)\right) := \sum_{n=0}^{N-1} l\left(\boldsymbol{x_n}, \boldsymbol{u_n}\right)$$

$$\text{s.t.}$$

$$\boldsymbol{x}_0 = \boldsymbol{x_{in}} \ \left(k\right)$$

$$\boldsymbol{x_{n+1}} = f_d \ \left(\boldsymbol{x_n}, \boldsymbol{u_n}\right)$$

$$\underline{\boldsymbol{x}} \leq \boldsymbol{x_n} \leq \bar{\boldsymbol{x}}$$

$$\underline{\boldsymbol{x}} \leq \boldsymbol{x_N} \leq \bar{\boldsymbol{x}}$$

$$\underline{\boldsymbol{u}} \leq \boldsymbol{u_n} \leq \bar{\boldsymbol{u}}$$

$$\boldsymbol{u}\left(\cdot\right) \ : [0, \ N-1] \tag{18}$$

where $\boldsymbol{u}(\cdot)$ indicates the control sequence; $\boldsymbol{x_{in}}$ is the initial value of the state vector, i.e., the value at the current time step k, obtained from the available sensor measurements and state estimators; the subscript n indicates the position of the step along $H_P = N\ T_s$; $\underline{\boldsymbol{x}}$ and $\bar{\boldsymbol{x}}$ are the lower and upper limits for $\boldsymbol{x}$, respectively; $\underline{\boldsymbol{u}}$ and $\bar{\boldsymbol{u}}$ are the lower and upper limits for $\boldsymbol{u}$, respectively; $\boldsymbol{x_{n+1}} = f_d\left(\boldsymbol{x_n}, \boldsymbol{u_n}\right)$ is the discretized version of (1); and $l(\boldsymbol{x_n}, \boldsymbol{u_n})$ is the stage cost function associated with each time step, which is defined as:

$$l\left(\boldsymbol{x_n}, \boldsymbol{u_n}\right) = \sum_{j=L,R} \Big[W_{u,\varepsilon_{\sigma_{x,F}}} \varepsilon^2_{\sigma_{x,Fj},n} + W_{u,\varepsilon_{\sigma_{x,R}}} \varepsilon^2_{\sigma_{x,Rj},n} + W_{u,\Delta T_{b,F}} \Delta T^2_{b,Fj,n} + W_{u,\Delta T_{b,R}} \Delta T^2_{b,Rj,n} \Big] \tag{19}$$

TABLE I
NMPC COST FUNCTION WEIGHTS

	$W_{u,\Delta T_{b,i}}$	$W_{u,\varepsilon_{\sigma_{x,i}}}$	
		Simulations	Experiments
Pre-NMPC with τ_{hb}	1	1.5×10^{9}	1×10^{12}
Pre-NMPC w/o τ_{hb}	1	1×10^{12}	1×10^{12}
NMPC with τ_{hb}	1	1.5×10^{9}	1×10^{12}
NMPC w/o τ_{hb}	1	1×10^{12}	1×10^{12}

where $W_{u,\varepsilon_{\sigma_{x,i}}}$ and $W_{u,\Delta T_{b,i}}$ are the cost function weights penalizing the slack variables and control action.

The constraints are:

$$-T_{b,drv,i} \leq \Delta T_{b,ij,n} \leq 0$$

$$\sigma_{x,ij,n} - \sigma_{x,thr,ij,n} + \varepsilon_{\sigma_{x,ij},n} \geq 0$$

$$\varepsilon_{\sigma_{x,ij},n} \geq 0. \tag{20}$$

The first line of (20) is a hard constraint that specifies the control action to be a reduction of the driver braking torque demand. The remaining conditions are soft constraints on the violation of the longitudinal slip ratio threshold $\sigma_{x,thr,ij,n}$, generated from predetermined tire force-slip lookup tables, to keep the slip close to the value corresponding to the maximum braking force for each friction factor $\mu_{ij,fut}$.

The controllers were implemented in the MATLAB/Simulink environment through the ACADO toolkit [20], with $T_s = 8$ ms (constrained by the solenoid valve limitations discussed in Section III-B), and an internal model discretization time step of 1 ms. Unless otherwise specified, the NMPC cost function weights have the values in Table I, providing a good response for the considered operating conditions.

E. Pre-Emptive PID ABS Controller

A pre-emptive PID ABS controller, "Pre-PID", is developed to allow a comparison with the proposed NMPCs. Independent PID modules are used for each corner, which track the longitudinal tire slip threshold $\sigma_{x,thr,ij}$ defined earlier for the NMPCs, with the error value $\sigma_{x,ij,error}$ sent to each PID controller being:

$$\sigma_{x,ij,error} = \sigma_{x,ij} - \sigma_{x,thr,ij} \tag{21}$$

The output of the PID modules is the friction braking torque $T_{b,ij}$ saturated to be positive and less than the driver braking torque demand, i.e., $0 \leq T_{b,ij} \leq T_{b,drv,i}$. The controller activates when the brake pedal is pressed and $\sigma_{x,ij} < \sigma_{x,thr,ij}$, and deactivates (with the integral term reset) when the brake pedal is released or the slip ratio magnitude remains below the threshold for a sufficiently long interval. Appropriate anti-windup conditions are used for the integral contribution.

The pre-emptive capability of "Pre-PID" comes from the V2X-obtained $\boldsymbol{\mu_{ij,fut}}(k)$ profiles in (13) and (14), which are used to generate $\sigma_{x,thr,ij}$, similar to the setup of the preview NMPCs. However, in (14), a different definition of $\boldsymbol{t_{fut}} = [t_{fut,0} + t_{PID,shift}]\ \mathbf{1}$ is used for "Pre-PID", reducing $\boldsymbol{t_{fut}}$ to a scalar, i.e., $N = 0$. Effectively, the constant time value $t_{PID,shift}$ shifts the entire tire–road friction factor map forward,

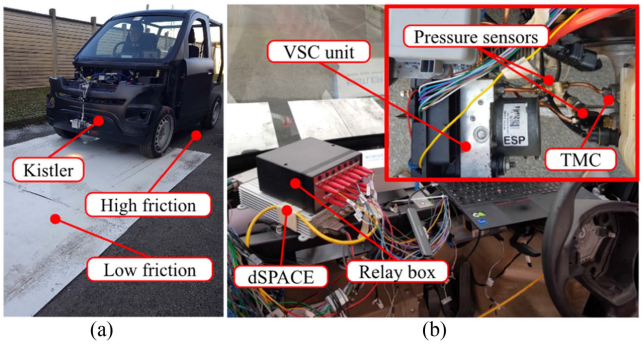

Fig. 2. (a) Prototype EV during a step change from high (dry tarmac) to low (water on white plastic boards) friction conditions; (b) Hardware components, including dSPACE MicroAutoBox II unit, custom-made relay box, and in the inset: modified VSC unit, pressure sensors, and TMC, located above the front axle.

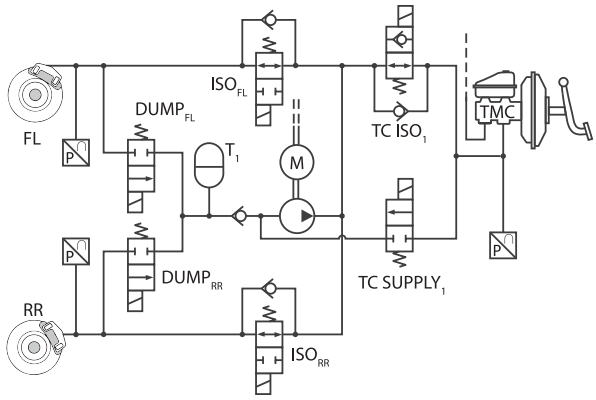

Fig. 3. Hydraulic schematic of the primary circuit of the modified VSC unit, serving the front left (FL) and rear right (RR) calipers. Pressure sensors are installed at the brake calipers and TMC.

TABLE II
MAIN VEHICLE PARAMETERS

Description	Parameters
Total vehicle mass m (kg)	677
Front semi-wheelbase l_F (m)	0.892
Rear semi-wheelbase l_R (m)	1.115
Wheel radius $R_{w,F/R}$ (m)	0.278
Wheel mass moment of inertia $J_{\omega,F/R}$ (kg·m^2)	1.5
Center of gravity height H_{CG} (m)	0.47

i.e., "Pre-PID" only uses the tire–road friction factor data ahead by $t_{PID,shift}$.

III. Case Study Vehicle

A. Hardware Components

The case study vehicle is a four-wheel-drive EV with a centralized onboard electric powertrain for each axle (see Fig. 2(a)), which was developed within the European Horizon 2020 Multi-Moby project [29]. The powertrains are connected to the wheels through single-speed transmissions, open differentials, half-shafts, and constant velocity joints. The main EV parameters are in Table II.

For this research, the EV was equipped with: i) individual wheel speed sensors; ii) a Kistler optical sensor to measure the longitudinal and lateral velocity components (see Fig. 2(a)), where the former was directly sent to the ABS; iii) an integrated PCAN global positioning system with IMU; iv) a dSPACE MicroAutoBox II system for the rapid control prototyping of the controllers (see Fig. 2(b)); and v) a modified commercial VSC unit (see the inset of Fig. 2(b)). The electronic control unit of the commercial VSC was replaced by a connection to the dSPACE board via relays to enable independent control of each digital solenoid valve and the motor pump in the hydraulic circuit in Fig. 3 from the dSPACE system. To allow feedback control of the individual caliper pressures, pressure sensors were installed at the output ports of the VSC unit, as well as one of the input ports connected to the TMC.

With respect to the measurement of the velocity components in ii), in a higher technology readiness level implementation, a state estimator similar to those in [21] and [30] would be used, with significant cost savings. To analyze the impact of the adopted approximation, the baseline version of the experimentally validated unscented Kalman filter in [30] was assessed along ABS tests with a conventional rule-based algorithm, in low tire–road friction conditions, by using the high-fidelity simulation model in Section IV-A. The results were contrasted with adopting the vehicle speed and slip ratio profiles directly from the model, i.e., without any estimation error. The closed-loop analysis highlighted relative variations of the root-mean-square (RMS) values amounting to 0.2% for V_x and 1% for $\sigma_{x,ij}$ between the two cases. This corresponds to a negligible impact of the estimation system on performance.

B. Low-Level Controller and Actuation System Characterization

A real-time low-level controller, see its pseudocode in Fig. 4, was developed in MATLAB/Simulink to allow closed-loop control of each brake caliper pressure during ABS/VSC activation events. Lines 1–5 distinguish between the case of VSC-induced pressure increase w.r.t. the TMC level and the case of pressure reduction, and express the actuation conditions of the TC ISO$_1$ and TC SUPPLY$_1$ valves of Fig. 3. Lines 6–11 represent the PI controller for the FL wheel with appropriate gain selection, which outputs the duty cycle $D_{FL} \in [-1, 1]$ for the pulse-width modulation (PWM) of the relevant ISO/DUMP valve. In the code, $t_{NMPC,last\_act,FL}$ is the instant at which the last activation of the NMPC ABS occurred in the considered corner. Appropriate anti-windup conditions were implemented for the integral term. Lines 12–16 account for the valve physical limits, which are usually the bottleneck of ABS controllers [31]. T_{min} is the minimum time before a new valve position request is allowed. T_{min} was determined by generating a unity amplitude square wave Act_v signal (saturated to $[0, 1]$) through the dSPACE system, and sending it to a relay, which would then activate/deactivate the solenoid of the respective valve. Based on the experiments, $T_{min} = 4$ ms, corresponding to a square wave period $T_{PWM} = 8$ ms, is the minimum value for reliable

```
% VSC or ABS activation
1  if (P_{b,FL,mod} > P_TMC or P_{b,RR,mod} > P_TMC) % VSC on
2      Act_{TC ISO 1} = Act_{TC SUPPLY 1} = 1
3  else % ABS on
4      Act_{TC ISO 1} = Act_{TC SUPPLY 1} = 0
5  end
% Switching of ISO and DUMP PI gains
6  if [P_{b,FL,mod} − P_{b,FL}] ≥ 0
7      k_p = k_{p,ISO}; k_i = k_{i,ISO} % use gains for ISO
8  else
9      k_p = k_{p,DUMP}; k_i = k_{i,DUMP} % use gains for DUMP
10 end
% PI control with duty cycle D_FL ∈ [−1,1] output
11 D_FL = k_p[P_{b,FL,mod} − P_{b,FL}]
        +k_i ∫_{t_{NMPC,last_act,FL}}^{t} [P_{b,FL,mod} − P_{b,FL}] dt
% Actuation physical limits, note: 2T_min ≤ T_PWM
12 if |D_FL| ∈ [0, T_min/(2T_PWM)) → D_FL.mod = 0 % Round down
13 if |D_FL| ∈ [T_min/(2T_PWM), T_min/T_PWM] → D_FL.mod = T_min/T_PWM % Round up
14 if |D_FL| ∈ (T_min/T_PWM, 1 − T_min/T_PWM) → D_FL.mod = |D_FL|
15 if |D_FL| ∈ [1 − T_min/T_PWM, 1 − T_min/(2T_PWM)]
                → D_FL.mod = 1 − T_min/T_PWM % Round down
16 if |D_FL| ∈ (1 − T_min/(2T_PWM), 1] → D_FL.mod = 1 % Round up
% Generate Act outputs
17 if D_FL ≥ 0 % Intensify or maintain pressure
18     D_FL.mod ∈ [0,1] → PWM with Act_{ISO,FL} ∈ [1,0]
       % Note inverted Act_{ISO,FL} output
19     Act_{DUMP,FL} = 0
20 else % Reduce pressure
21     D_FL.mod ∈ [0,1] → PWM with Act_{DUMP,FL} ∈ [0,1]
22     Act_{ISO,FL} = 1
23 end
24 repeat lines 6 to 23, replacing _FL with _RR
```

Fig. 4. Pseudocode of the low-level algorithm for primary circuit (FL/RR) actuation.

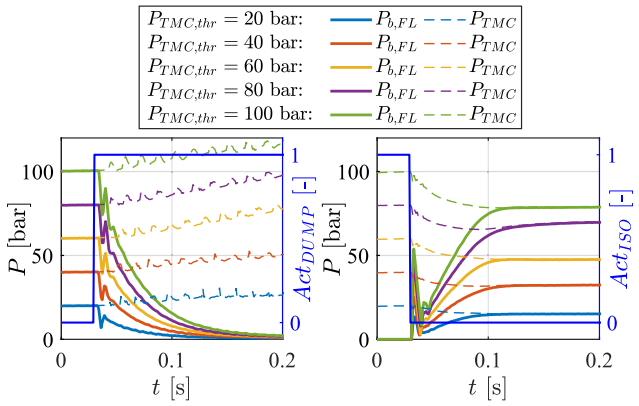

Fig. 5. Experimentally measured maximum pressure reduction and pressure increase performance for the FL caliper for different $P_{TMC,thr}$ setpoints.

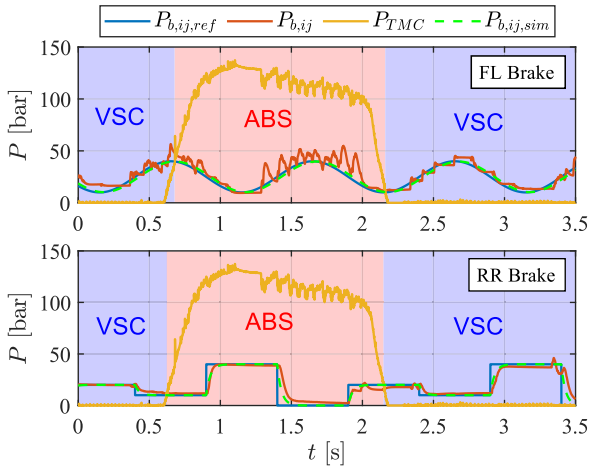

Fig. 6. Experimental results of the low-level feedback controller for the primary brake circuit.

operation of all ISO and DUMP valves. Below T_{min}, some of the brake caliper pressure sensors do not detect pressure variations during the square wave switching, i.e., the valve does not respond to the control input. Therefore, if the PI-generated duty cycle D_{FL} leads to PWM on-times or off-times that are shorter than T_{min}, lines 12–16 round them to 0 or T_{min}, resulting in $D_{FL,mod} \in \{0,\ 0.5,\ 1\}$ for the selected PWM operation at 8 ms. Lines 17–23 generate the valve outputs. For example, in line 18, a duty cycle $D_{FL.mod}$ in the $[0, 1]$ range leads to an on-time $T_{ISO,FL,on} = [1 - D_{FL,mod}]\ T_{PWM}$ for the normally open (NO) ISO_{FL} valve, during which $Act_{ISO,FL} = 1$. Concurrently, line 19 ensures that the normally closed (NC) DUMP_{FL} valve stays closed.

Fig. 5 reports the maximum pressure reduction and pressure increase performance of the hydraulic system, corresponding to the full activation of the DUMP_{FL} (left subplot) and ISO_{FL} (right subplot) valves, for different values of TMC pressure ($P_{TMC,thr}$) at which the valve is activated. The corresponding average fall (from 90% to 10% of the initial caliper pressure) and rise (from 10% to 90% of the steady-state pressure) times are 76 and 54 ms, with a moderate variation, corresponding to less than 10%, depending on $P_{TMC,thr}$.

Fig. 6 is an example of experimental characterization of the low-level controller. Different reference profiles were simultaneously imposed for the two primary circuit calipers, i.e., $P_{b,FL,ref} = P_{b,FL,mod}$ is a sinusoidal waveform, whereas $P_{b,RR,ref} = P_{b,RR,mod}$ is a sequence of steps. The measured pressures of both calipers highlight good tracking during both VSC and ABS actuation.

As per (11), two of the proposed NMPCs consider the brake actuation dynamics. The time constant τ_{hb} (i.e., the time for the system step response to reach 63.2% of its final asymptotic value) was experimentally determined by providing the low-level controller with a reference pressure profile consisting of a sequence of step changes from low-to-high pressure and vice versa, and measuring the corresponding $P_{b,ij}$ response. $\tau_{hb} = 30$ ms was determined by averaging the resulting values. In Fig. 6, the simulated first-order pressure profile $P_{b,ij,sim}$ matches well with the measurements, despite the simplicity of the model, which neglects the typical low-amplitude pressure oscillations of the physical actuation system.

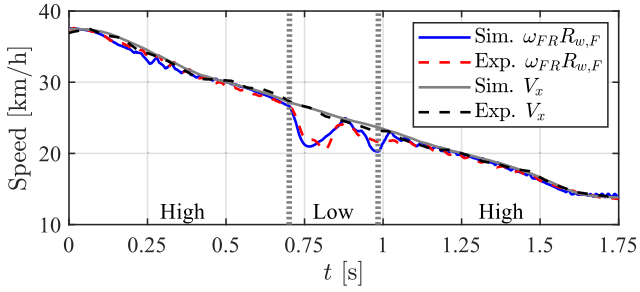

Fig. 7. Example of experimental validation of the vehicle simulation model along a braking test with abrupt tire–road friction transitions, see the vertical dotted lines that separate the different friction regions.

IV. Simulation Results

A. Simulation Model Validation

A high-fidelity simulation model of the case study EV was implemented in the MATLAB/Simulink–IPG CarMaker environment, including a nonlinear MF tire model with variable relaxation length [32]. Preliminary experimental tests were performed with the non-pre-emptive NMPC, e.g., braking with an average $|a_x|$ of $\sim$4 m/s^2 on a surface with abrupt high-to-low and low-to-high tire–road friction transitions (see Fig. 7).

For validation, the recorded experimental brake pressures were sent to the simulation model along the same scenario, which implies significant longitudinal tire slip and wheel dynamics in the low-friction section. The good overlap of the simulated and experimental V_x and $\omega_{ij}R_{w,i}$ profiles makes the model a useful tool for control system analysis.

B. Sensitivity to the Actuation Dynamics

The sensitivity of the nominal performance of the four controllers in Section II-A to the variation of τ_{hb} (15, 30, 45, and 60 ms) is assessed during an intense braking test (with $|a_x|$ exceeding 8.5 m/s^2 in the high-friction section) with an extreme high-to-low friction step (μ falling from 1 to 0.2), from an initial speed of 40 km/h. In all simulations, τ_{hb} is the same in the NMPC prediction model and the model for control system assessment. In the high-friction section, there is no ABS activation. Two H_P values are considered: i) 40 ms, which corresponds to $N = 5$, and is the longest real-time implementable H_P for the "Pre-NMPC" configurations on the available dSPACE MicroAutoBox II system (though more powerful hardware is available on the market); and ii) 120 ms, corresponding to $N = 15$. The cost function weights are optimized for the specific test and plant properties.

Fig. 8 includes the slip ratio profiles for the FR wheel, as a representative example. For the same simulations, Fig. 9 reports: a) RMSE $\sigma_{x,FR}$, the RMS value of the slip ratio error $\sigma_{x,FR} - \sigma_{x,thr,FR}$ in the low-friction section; and b) the peak value of $|\sigma_{x,FR}|$. With respect to the non-pre-emptive configurations, the first peak of $\sigma_{x,FR}$ is substantially the same for "NMPC w/o τ_{hb}" and "NMPC with τ_{hb}". In the low-friction section, the controllers embedding the actuation dynamics manage to better damp the low-amplitude oscillations of $\sigma_{x,FR}$ around $\sigma_{x,thr,FR}$, and approach steady-state quicker. As the algorithms

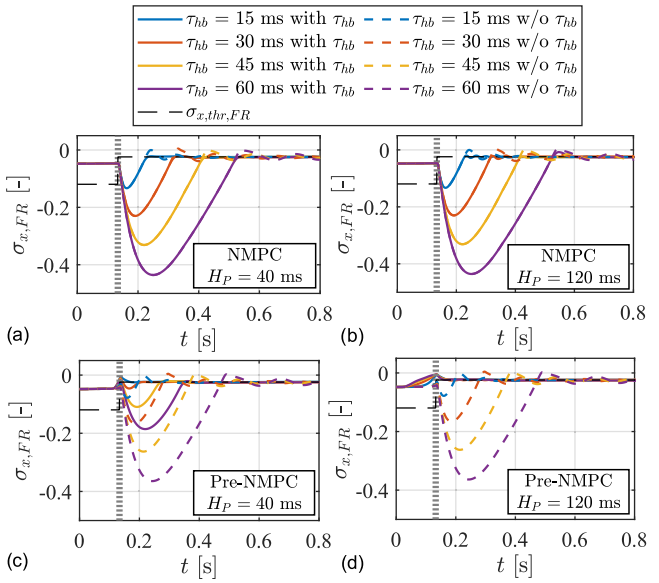

Fig. 8. Simulation results in terms of $\sigma_{x,FR}$ profiles for (a) "NMPC with τ_{hb}" and "NMPC w/o τ_{hb}", with $H_P = 40$ ms; (b) "NMPC with τ_{hb}" and "NMPC w/o τ_{hb}", with $H_P = 120$ ms; (c) "Pre-NMPC with τ_{hb}" and "Pre-NMPC w/o τ_{hb}", with $H_P = 40$ ms; and (d) "Pre-NMPC with τ_{hb}" and "Pre-NMPC w/o τ_{hb}", with $H_P = 120$ ms.

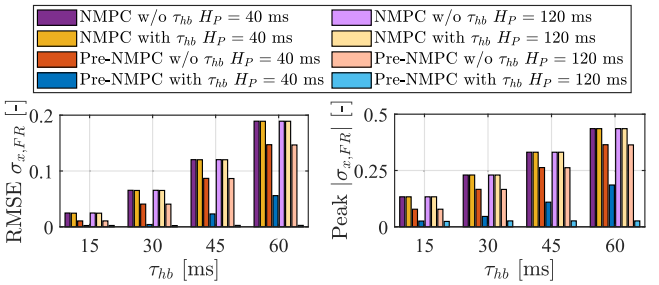

Fig. 9. Histograms in terms of RMSE and peak of $\sigma_{x,FR}$, for different values of τ_{hb}, $H_P = 40$ ms and 120 ms, for the considered NMPC configurations.

are not aware of the upcoming tire–road friction transition, the larger the τ_{hb}, the worse the controller performance, see the increasing magnitude of the negative $\sigma_{x,FR}$ peaks as a function of τ_{hb}. Interestingly, H_P has negligible effect on the results, since the reference pressure is reduced only after the wheel crosses the μ-jump, independently from H_P.

"Pre-NMPC w/o τ_{hb}" behaves similarly, although marginally better, to the non-pre-emptive NMPCs, with large slip ratio peaks. In fact, as the controller is unaware of the actuation dynamics, it deems that the hydraulics can instantly reduce the braking torque, and thus, although knowing the friction step sufficiently in advance, it only requests a braking torque reduction immediately before the μ-jump. Therefore, H_P has no tangible effect on the "Pre-NMPC w/o τ_{hb}" response. In contrast, despite the simplicity of its internal actuation model, "Pre-NMPC with τ_{hb}" reduces the braking torque well in advance of the μ-jump, resulting in a substantially complete compensation of the first $\sigma_{x,FR}$ peak, in the configurations with $H_P = 120$ ms. For

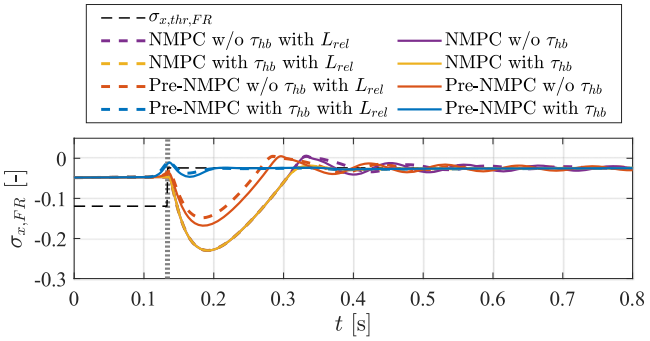

Fig. 10. Simulation results in terms of $\sigma_{x,FR}$ profiles, showing the effect of tire force relaxation for $H_P = 40$ ms.

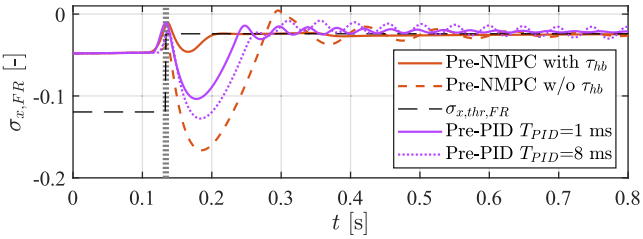

Fig. 11. Simulation results in terms of $\sigma_{x,FR}$ profiles, comparing the "Pre-NMPC" and "Pre-PID" configurations.

$H_P = 40$ ms, the $\sigma_{x,FR}$ peaks can still be observed, though they are significantly smaller than for "Pre-NMPC w/o τ_{hb}". This is caused by the fact that H_P is of comparable magnitude to τ_{hb}, with the $\tau_{hb} = 60$ ms case performing the worst.

The trends in Fig. 9 are the same for the RMSE and peak values, i.e., increasing τ_{hb} leads to worse performance, except for "Pre-NMPC with τ_{hb}" for $H_P = 120$ ms, which provides consistently excellent results, regardless of the actuation hardware capabilities.

C. Effect of Tire Relaxation in the Internal Model

The tire dynamics are added to the NMPC internal model to study their effect on the controller response. The state vector for "Pre-NMPC with τ_{hb}" and "NMPC with τ_{hb}" becomes:

$$\boldsymbol{x} = [\omega_{FL}, \omega_{FR}, \omega_{RL}, \omega_{RR}, T_{b,FL}, T_{b,FR}, T_{b,RL}, T_{b,RR}, \sigma_{d,FL}, \sigma_{d,FR}, \sigma_{d,RL}, \sigma_{d,RR}] \tag{22}$$

while the NMPCs neglecting the actuation dynamics omit the $T_{b,ij}$ terms. The additional states associated with tire relaxation are the delayed longitudinal slip ratios $\sigma_{d,ij}$, whose dynamics are given by [28]:

$$\dot{\sigma}_{d,ij} = \frac{V_x}{L_{rel}} \left[\sigma_{x,ij} - \sigma_{d,ij}\right] \tag{23}$$

where L_{rel} is the relaxation length. Fig. 10 shows the comparison between the earlier results of the case "$\tau_{hb} = 30$ ms with τ_{hb}" in Fig. 8, and the corresponding controllers considering tire relaxation ("with L_{rel}"). The controllers without preview do not experience any benefit from the tire dynamics, as they respond similarly, with the reduction of the reference braking torque immediately after the μ-jump. In contrast, for the "Pre-NMPC" cases, there are minor improvements in terms of $\sigma_{x,FR}$ peaks when tire relaxation is accounted for, e.g., compare "Pre-NMPC with τ_{hb} with L_{rel}" and "Pre-NMPC with τ_{hb}". However, the inclusion of the actuator dynamics in the internal model, see "Pre-NMPC with τ_{hb}" and "Pre-NMPC w/o τ_{hb}", brings a much greater improvement, as the HAB dynamic effects dominate over the transient tire behavior. Therefore, the implementations of the following sections will not include the tire relaxation effect in the NMPC models, to reduce the computational burden.

D. Comparison With the Pre-Emptive PID ABS Controller

Fig. 11 shows a comparison of the "Pre-NMPC" configurations with two versions of the benchmarking "Pre-PID" controllers. The first "Pre-PID" is a best-case scenario controller, operating with an implementation step $T_{PID} = 1$ ms, whereas the second "Pre-PID" has $T_{PID} = 8$ ms, which is the configuration physically implementable on the case study vehicle, based on the valve limitations discussed in Section III-B. $t_{PID,shift}$ was tuned to be 20 ms, such that the pre-emptive behavior of "Pre-PID" (immediately preceding the μ-jump) is similar to the one of "Pre-NMPC with τ_{hb}", i.e., this "Pre-PID" tuning brings the best performance. From the figure, "Pre-NMPC with τ_{hb}" has the smallest $\sigma_{x,FR}$ peak, followed by "Pre-PID $T_{PID}=$ 1 ms", "Pre-PID $T_{PID} = 8$ ms", and finally "Pre-NMPC w/o τ_{hb}". The "Pre-PID" controllers perform better than "Pre-NMPC w/o τ_{hb}" because an appropriate value of $t_{PID,shift}$ relative to τ_{hb} effectively allows consideration of the actuation dynamics before the μ-jump. However, both "Pre-PID" implementations are affected by a slower decay of the oscillations after the friction jump, similar to the controllers "w/o τ_{hb}" in Fig. 8. This is due to the actuator response deriving from τ_{hb}. "Pre-PID $T_{PID} = 8$ ms" brings a worse $\sigma_{x,FR}$ peak and more persistent oscillations compared to "Pre-PID $T_{PID} = 1$ ms", because the longer T_{PID} behaves like an additional time delay. "Pre-NMPC with τ_{hb}" provides the best performance with negligible oscillations.

A non-pre-emptive PID was also simulated, i.e., with $t_{PID,shift} = 0$, which performed the worst. In fact, the first $\sigma_{x,FR}$ peak is identical to the one of "NMPC w/o τ_{hb}", as the torque reduction occurs only after the friction step, and the following oscillations are characterized by a very slow decay.

E. Robustness Analyses

Although uncertainty is not considered explicitly in the proposed NMPC problem formulations, the inherent robustness of model predictive control has been widely discussed [33]. Nevertheless, for completeness, a simulation-based Monte Carlo analysis of the NMPCs is carried out along high-to-low friction braking tests to verify the robustness of the real-time controllers ($H_P = 40$ ms) w.r.t. parameter variations. The considered parameters are as follows:

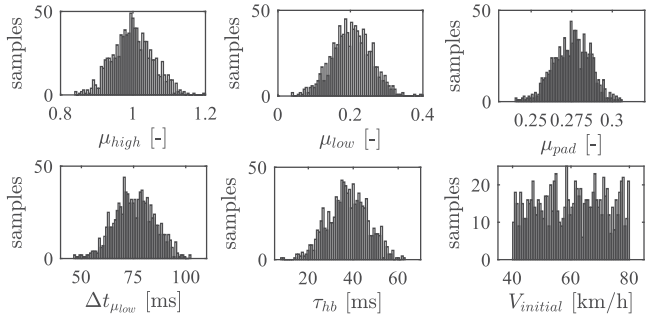

Fig. 12. Parameters distribution for the Monte Carlo analysis.

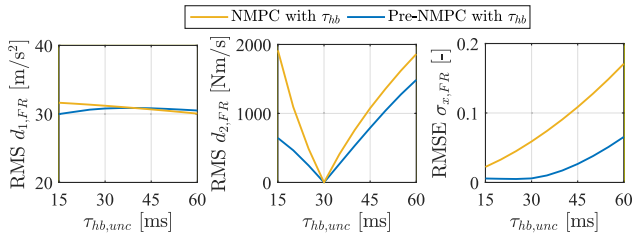

Fig. 13. RMS values of $d_{1,FR}$ and $d_{2,FR}$, and RMSE value of $\sigma_{x,FR}$, for "NMPC with τ_{hb}" and "Pre-NMPC with τ_{hb}", during ABS tests with different $\tau_{hb,unc}$ values.

TABLE III
RESULTS OF MONTE CARLO SIMULATIONS

Controller	Wheel locking $\sigma_{x,ij}=-1$	Underbraking $\sigma_{x,ij}\geq 0$	
	$\Delta_{thr}=5\%$	$\Delta_{thr}=5\%$	$\Delta_{thr}=10\%$
Pre-NMPC with τ_{hb}	0%	3%	0.3%
Pre-NMPC w/o τ_{hb}	0%	0.1%	0%
NMPC with τ_{hb}	0%	1.3%	0%
NMPC w/o τ_{hb}	0%	0.1%	0%

1) The value of the friction factor μ_{high} in the high-friction section of the road scenario, which is imposed in the CarMaker model, whereas the controllers receive a constant $\mu_{high}=1$.
2) The value of the friction factor μ_{low}, which is imposed in the CarMaker model in the low-friction section of the scenario.
3) The pure time delay $\Delta t_{\mu_{low}}$ in the communication of the actual value of μ_{low} to the controller, rather than its approximated value equal to 0.2 from V2X, whereas the plant model sees the correct μ_{low} without delays (this represents a scenario with erroneous V2X friction data, subsequently corrected with data from onboard state estimators after a short delay).
4) The HAB time constant τ_{hb}, which modifies the plant dynamics, but is kept constant and equal to 30 ms in the prediction models.
5) The friction coefficient between the brake pads and disc μ_{pad} used in the plant model (varied according to the indications in [34]) while it is kept constant within the controllers.
6) The initial vehicle speed $V_{initial}$, which is correctly provided to the plant and controllers.

In total, 1000 scenarios were simulated with randomly selected samples from the distributions in Fig. 12. The robustness evaluation was inspired by the European regulation for ABS-equipped passenger cars [35], which permits only short intervals of wheel locking. The results are in Table III, which reports the percentages of tests in which: a) locking ($\sigma_{x,ij}=-1$) occurs for at least one wheel for a total duration exceeding the percentage threshold Δ_{thr} of the time in which the ABS is active on the same corner; and b) significant underbraking ($\sigma_{x,ij}\geq 0$) occurs for at least one wheel for a total duration computed according to a). Two Δ_{ths} values, i.e., 5% and 10%, were used. None of the controllers experiences wheel locking exceeding $\Delta_{thr}=5\%$ in any scenario. When present, the percentages of underbraking instances are small and deemed acceptable.

A further robustness analysis is carried out by considering the plant as a mismatched system, according to the formulation in [36]. In fact, by substituting (4) into the time derivative of (7) and considering the actuation dynamics, the system can be described by:

$$\begin{cases} \dot{\sigma}_{x,ij} = \frac{1}{V_x}\left[-\frac{R_{w,i}T_{b,ij}}{J_{\omega,i}} + d_{1,ij}\right] \\ \dot{T}_{b,ij} = \frac{T_{b,drv,i}+\Delta T_{b,ij}-T_{b,ij}}{\tau_{hb}} + d_{2,ij} \end{cases} \tag{24}$$

where the terms $d_{1,ij}$ and $d_{2,ij}$ are disturbances, respectively, related to the wheel and actuation dynamics uncertainties:

$$\begin{cases} d_{1,ij} = -\frac{F_{x,ij}R_{w,i}^2}{J_{\omega,i}} - \dot{V}_x\left[1+\sigma_{x,ij}\right] \\ d_{2,ij} = \frac{T_{b,drv,i}+\Delta T_{b,ij}-T_{b,ij}}{\tau_{hb,unc}} - \frac{T_{b,drv,i}+\Delta T_{b,ij}-T_{b,ij}}{\tau_{hb}} \end{cases} \tag{25}$$

where $\tau_{hb,unc}$ is the uncertain time constant of the brake actuators, i.e., the one set in the CarMaker model, for which 10 discrete values from 15 to 60 ms are selected. τ_{hb} is the nominal value, equal to 30 ms, used in the internal model. The scenario is the same used for the sensitivity analysis in Section IV-B.

Fig. 13 shows that: i) the actuation dynamics disturbance $d_{2,FR}$ is significantly affected by $\tau_{hb,unc}$, as expected based on (25); ii) the resulting system dynamics disturbance $d_{1,FR}$ only marginally varies with $\tau_{hb,unc}$, which confirms the good robustness level of both controllers; and iii) more importantly, $\sigma_{x,FR}$ is always lower for "Pre-NMPC with τ_{hb}", which is also associated with a smaller sensitivity of the slip ratio error to $\tau_{hb,unc}$. Similar trends are observed for the other vehicle corners.

V. PROOF-OF-CONCEPT VEHICLE EXPERIMENTS

A. Experimental Setup

The proof-of-concept experiments evaluate the passive case ("Passive"), i.e., without ABS, the real-time setting of the four NMPC and "Pre-PID". A μ-jump scenario is set up (see Fig. 2(a)), where the high-friction section is dry tarmac, and the low-friction section is achieved through smooth plastic boards covered with water. The tire–road friction factor in spatial coordinates is uploaded into the dSPACE MicroAutoBox II system beforehand to represent the V2X input (the generation and transmission of V2X data are outside the scope of this research). Given the short traveled distance, the vehicle position is obtained through integration of the vehicle speed profile from the Kistler

Fig. 14. Image sequence (from left to right) of a production M1 vehicle equipped with its factory-installed ABS, during the extreme high-to-low tire–road friction step test. The red markings on the tire highlight that the wheel does not rotate (i.e., it is locked) in the low-μ section, represented by the wet white plastic boards (the edge of the white board in the bottom right of each image can be used as a static visual reference).

sensor. In the tests, the human driver accelerates the EV to ∼40 km/h, applies a significant brake pedal force in the high-friction section (corresponding to a P_{TMC} level of ∼140 bar), ∼2.2 m before the transition to low friction, and maintains it until the vehicle comes to a standstill. For simplicity, the proposed ABS controllers are experimentally implemented only on the front axle, as a proof-of-concept. During braking, the rear caliper pressures are maintained at 10 bar, below the wheel locking threshold, through the closed-loop low-level controller.

The extreme severity of the scenario was verified by performing the maneuver with a production M1 vehicle with its standard equipment ABS. The commercial ABS is active during the whole test, generating the typical brake pedal oscillations, but cannot handle the sudden transition to the low-μ section, throughout which the front wheels remain locked (see Fig. 14).

B. High-to-Low Friction Scenario

Fig. 15 reports the experimental $P_{b,FR}$ (subplots (a) and (b)) and $\sigma_{x,FR}$ (subplot (c)) profiles for tests in which the brake pedal force is applied shortly before $t = 0$, and the μ-jump occurs at $t \approx 0.25$ s on both front wheels. For "Passive", as $P_{b,FR} \approx P_{TMC}$ (out of scale in the subplot), $\sigma_{x,FR}$ reaches -1, indicating wheel locking in both the high- and low-friction sections. All controllers activate during the brake application, by maintaining an average $P_{b,FR}$ of ∼30 bar in the high-friction section, which enables $\sigma_{x,FR}$ to meet the $\sigma_{x,thr,FR}$-based constraint with marginal oscillations. Interestingly, in the high-μ phase, the controllers neglecting the actuation dynamics output $P_{b,FR,mod}$ profiles with significantly smaller oscillations than those embedding actuation delays. In fact, the latter, being aware of the filtering effect of the HAB hardware and low-level controller, are rather aggressive in modulating the reference, to obtain the required moderate variation of the actual pressure $P_{b,FR}$.

Immediately after the μ-jump, the non-pre-emptive controllers request a zero value of $P_{b,FR,mod}$, as $\sigma_{x,FR}$ rapidly reaches the –0.6 to –0.8 range. In "Pre-NMPC w/o τ_{hb}", the pressure reduction is requested immediately before the tire–road friction step change. Nevertheless, the reduction is demanded too late; therefore, $\sigma_{x,FR}$ also rapidly falls to ~ -0.6, and the response is similar to those of the non-pre-emptive controllers.

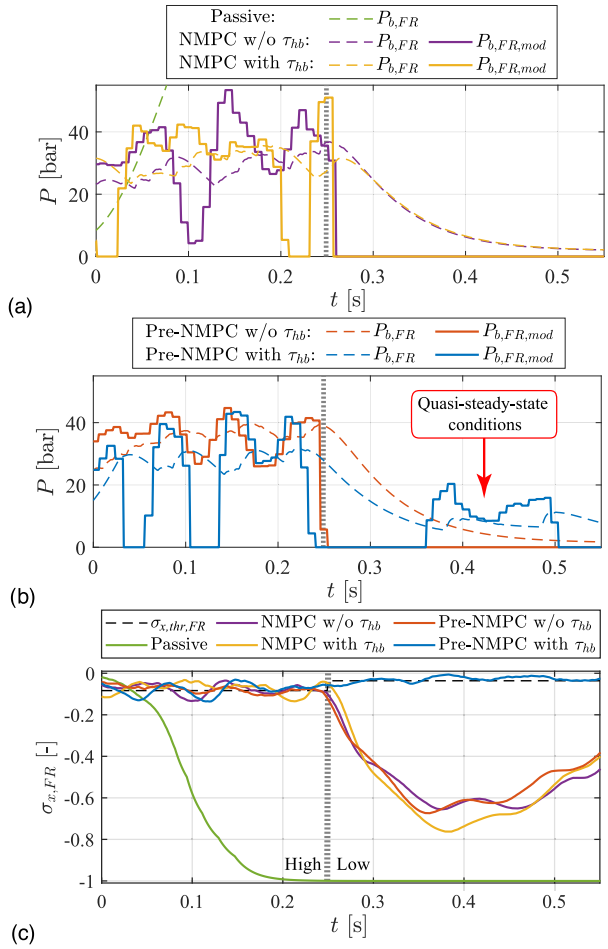

Fig. 15. Experimental test results along the high-to-low friction ABS test from 40 km/h: (a) $\boldsymbol{P_{b,FR}}$ and $\boldsymbol{P_{b,FR,mod}}$ profiles for "Passive", "NMPC w/o $\boldsymbol{\tau_{hb}}$", and "NMPC with $\boldsymbol{\tau_{hb}}$"; (b) $\boldsymbol{P_{b,FR}}$ and $\boldsymbol{P_{b,FR,mod}}$ profiles for "Pre-NMPC w/o $\boldsymbol{\tau_{hb}}$", and "Pre-NMPC with $\boldsymbol{\tau_{hb}}$"; and (c) $\boldsymbol{\sigma_{x,FR}}$ profiles for all configurations, together with the corresponding $\boldsymbol{\sigma_{x,thr,FR}}$ time plot.

As "Pre-NMPC with τ_{hb}" has preview capabilities and is aware of the actuation delays, it pre-emptively reduces $P_{b,FR}$ before the μ-jump. Hence, $\sigma_{x,FR}$ is able to substantially meet the soft constraint defined by $\sigma_{x,thr,FR}$ immediately after the transition to the low-friction section, after which the system reaches quasi-steady-state conditions, and the caliper pressure is regulated at 10 to 15 bar. To visually confirm the excellent performance of the most advanced algorithm, in contrast with the behavior of the conventional ABS system (in Fig. 14), Fig. 16 reports the image sequence of the prototype EV with "Pre-NMPC with τ_{hb}", in which the front wheel does not tend to lock after the tire–road friction drop.

C. NMPC Robustness and Comparison With "Pre-PID"

Fig. 17(a) refers to an induced mass mismatch, amounting to ±100 kg, between the NMPC internal model and the actual vehicle. The controllers with the mismatch perform similarly to their respective nominal counterparts. The nominal

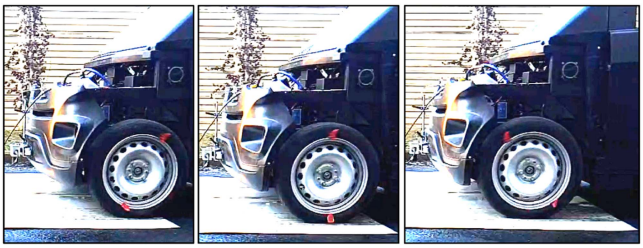

Fig. 16. Image sequence (from left to right) of the prototype EV with "Pre-NMPC with τ_{hb}", during the same high-to-low tire–road friction step change test as in Fig. 14. The wheel does not tend to lock, and meets the soft constraint defined by the slip ratio threshold.

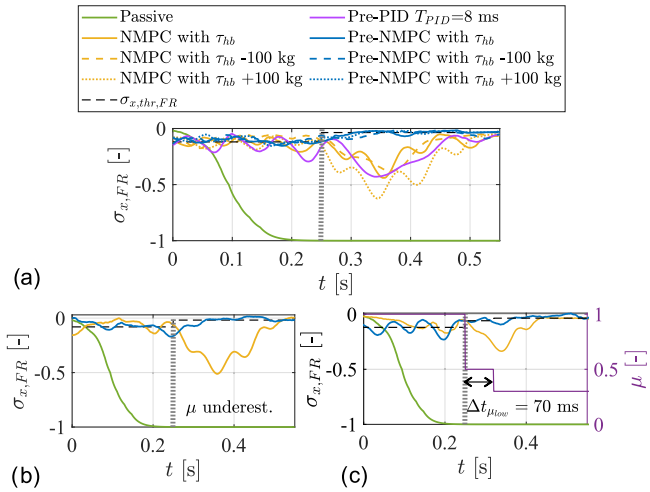

Fig. 17. Experimental results along high-to-low friction ABS tests from 40 km/h, with mismatches between the NMPC internal models and the actual vehicle: (a) $\sigma_{x,FR}$ profiles for "Passive", "NMPC with τ_{hb}", and "Pre-NMPC with τ_{hb}" with mass mismatches, and comparison with "Pre-PID"; (b) $\sigma_{x,FR}$ profiles in presence of underestimation of the friction factor; and (c) $\sigma_{x,FR}$ profiles in presence of friction data communication delay $\Delta t_{\mu_{low}}$.

"NMPC with τ_{hb}" and "Pre-NMPC with τ_{hb}" results in Fig. 17 differ from those in Fig. 15, as Fig. 17 tests were performed in an independent session, with higher values of the friction coefficients for both the high and low friction sections. In addition, Fig. 17(a) shows a comparison with "Pre-PID" with $T_{PID} = 8$ ms, where "Pre-NMPC with τ_{hb}"—even when including parametrization errors—outperforms "Pre-PID". In Fig. 17(b), the friction factors from V2X are underestimated in both the high- and low-friction sections, in a similar setup to the Monte Carlo simulations in Section IV-E, whereas in Fig. 17(c), the low-friction factor from V2X is initially an erroneous 0.5, see the right y-axis, which is updated to the correct value of 0.3 after $\Delta t_{\mu_{low}}$. Importantly, when faced with friction factor errors, the NMPCs are relatively robust, with similar performance to the nominal controllers in Fig. 17(a).

D. Split-μ Scenario

Fig. 18 refers to emergency braking experiments on a split-μ road, where the right wheels encounter a high-to-low friction

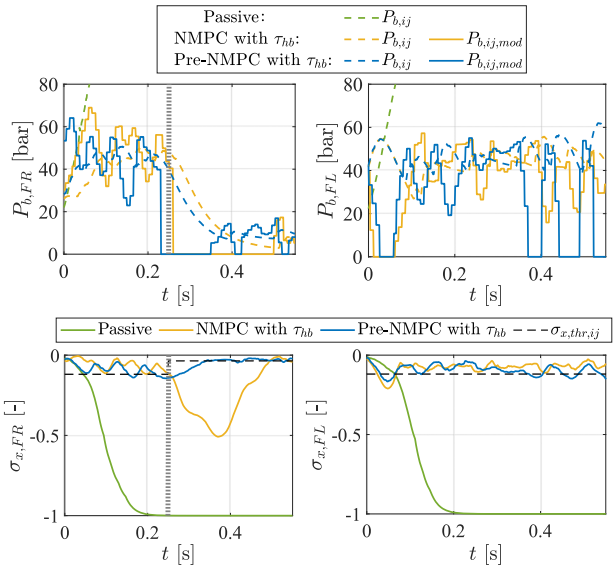

Fig. 18. Experimental ABS results from 40 km/h, with a high-to-low friction step on the right wheel, and constant high friction on the left one.

step while the left ones stay in high friction. As expected, on the right wheel, the NMPCs behave similarly to Fig. 17(a), whereas on the left corner, the brake pressure oscillates around ∼45 bar, to maintain $\sigma_{x,FL}$ close to $\sigma_{x,thr,FL}$.

VI. Conclusion

This study presented novel ABS algorithms with preview of the expected tire–road friction factor ahead for next-generation V2X-connected vehicles. The controllers were experimentally implemented on an EV demonstrator with a commercial hydraulic unit for stability control actuation. The main conclusions are as follows:

1) Extending the prediction horizon does not have any substantial effect on the performances of the non-pre-emptive controllers and the pre-emptive controller neglecting the actuation dynamics. However, to achieve the full potential benefit of the pre-emptive NMPC considering the actuation transients, the prediction horizon should be larger than the time constant of the actuation system.
2) The Monte Carlo simulations and experiments with prediction model mismatches and disturbances highlight that the presence of preview does not compromise performance robustness.
3) The pre-emptive NMPC ABS considering the actuation dynamics can be implemented in real time in implicit form on the available control hardware, with meaningful parameterizations in terms of time step and prediction horizon.
4) The simulations and proof-of-concept experiments highlight the benefit of the most advanced formulation, including preview and consideration of actuation dynamics, in maneuvers with extreme high-to-low friction transitions, also in comparison with a benchmarking pre-emptive PID controller. In fact, the preview information enables

a pre-emptive reduction of the reference caliper pressure, which brings a timely decrease of the actual braking torque. Such control input effectively compensates for the slip ratio peak that is typical of the operation of feedback ABS controllers without preview during the considered tests, and reduces the RMS value of the slip ratio error.

5) The inclusion of either the actuation dynamics in the controller without preview or the preview in the algorithm neglecting the actuation dynamics does not bring any significant benefit. Only the concurrent consideration of both effects leads to a major performance enhancement. On the contrary, tire relaxation effects can be neglected in the prediction model.

Future developments will include the following:

1) A single centralized pre-emptive NMPC ABS implementation instead of independent NMPCs for each wheel corner.
2) The integration of the pre-emptive NMPC ABS with the VSC function and required state estimators.
3) Theoretical robustness analyses of the proposed controllers.
4) The evaluation of the practical implementation aspects of the required V2X technology, including costs.

References

[1] J. Lawes, *Car Brakes: A Guide to Upgrading, Repair and Maintenance*. Ramsbury, U.K.: Crowood Press, 2014.

[2] K. Reif, *Brakes, Brake Control and Driver Assistance Systems: Function, Regulation and Components*. Wiesbaden, Germany: Springer-Vieweg, 2014.

[3] S. M. Savaresi and M. Tanelli, *Active Braking Control Systems Design for Vehicles*. London, U.K.: Springer-Verlag, 2010.

[4] F. Pretagostini, L. Ferranti, G. Berardo, V. Ivanov, and B. Shyrokau, "Survey on wheel slip control design strategies, evaluation and application to antilock braking systems," *IEEE Access*, vol. 8, pp. 10951–10970, 2020.

[5] S. B. Phadke, P. D. Shendge, and V. S. Wanaskar, "Control of antilock braking systems using disturbance observer with a novel nonlinear sliding surface," *IEEE Trans. Ind. Electron.*, vol. 67, no. 8, pp. 6815–6823, Aug. 2020.

[6] M. Choi, K. Choi, M. Cho, M. Lee, and K. Kim, "Chattering reduction of sliding mode control via nonlinear disturbance observer for anti-lock braking system and verification with CarSim simulation," *Int. J. Automot. Technol.*, vol. 24, no. 4, pp. 1141–1149, 2023.

[7] S. Li, L. Guo, B. Zhang, X. Lu, G. Cui, and J. Dou, "MPC-based slip control system for in-wheel-motor drive EV," *Proc. 5th IFAC Conf. Engine Powertrain Control, Simul. Model. E-COSM*, vol. 51, no. 31, pp. 578–582, 2018.

[8] M. S. Basrah, E. Siampis, E. Velenis, D. Cao, and S. Longo, "Wheel slip control with torque blending using linear and nonlinear model predictive control," *Veh. Syst. Dyn.*, vol. 55, no. 11, pp. 1665–1685, 2017.

[9] Y. Ma, J. Zhao, H. Zhao, C. Lu, and H. Chen, "MPC-based slip ratio control for electric vehicle considering road roughness," *IEEE Access*, vol. 7, pp. 52405–52413, 2019.

[10] V. M. Arricale, A. Genovese, A. S. Tomar, K. Kural, and A. Sakhnevych, "Non-linear model of predictive control-based slip control ABS including tyre tread thermal dynamics," *Appl. Mechanics*, vol. 3, no. 3, pp. 855–888, 2022.

[11] R. He and L. Yuan, "An improved nonlinear predictive control strategy enhanced by fractional order extremum seeking control of the antilock braking system of a vehicle," *IEEE Access*, vol. 8, pp. 168576–168588, 2020.

[12] P. V. Gaurkar, A. Challa, K. Ramakrushnan, S. C. Subramanian, G. Vivekanandan, and S. Sivaram, "Model predictive control of wheel slip towards antilock brake system using convex optimization," in *Proc. Int. Conf. Commun. Syst. Netw.*, 2021, pp. 644–649.

[13] D. Tavernini et al., "An explicit nonlinear model predictive ABS controller for electro-hydraulic braking systems," *IEEE Trans. Ind. Electron.*, vol. 67, no. 5, pp. 3990–4001, May 2020.

[14] Z. He, Q. Shi, Y. Wei, B. Gao, B. Zhu, and L. He, "A model predictive control approach with slip ratio estimation for electric motor antilock braking of battery electric vehicle," *IEEE Trans. Ind. Electron.*, vol. 69, no. 9, pp. 9225–9234, Sep. 2022.

[15] C. Satzger and R. de Castro, "Predictive brake control for electric vehicles," *IEEE Trans. Veh. Technol.*, vol. 67, no. 2, pp. 977–990, Feb. 2018.

[16] A. Scamarcio et al., "Predictive antijerk and traction control for V2X connected electric vehicles with central motor and open differential," *IEEE Trans. Veh. Technol.*, vol. 72, no. 6, pp. 7221–7239, Jun. 2023.

[17] G. Tavolo, K. M. So, D. Tavernini, P. Perlo, and A. Sorniotti, "Nonlinear model predictive control for preview-based traction control," in *Proc. 15th Int. Symp. Adv. Veh. Control*, 2022, pp. 1–6.

[18] K. M. So et al., "Novel pre-emptive control solutions for V2X connected electric vehicles," in *Proc. Transport Res. Arena Conf.*, 2022, pp. 1–8.

[19] G. Guastadisegni et al., "Vehicle stability control through pre-emptive braking," *Int. J. Automot. Technol.*, vol. 24, no. 2, pp. 347–365, 2023.

[20] B. Houska, H. J. Ferreau, and M. Diehl, "An auto-generated real-time iteration algorithm for nonlinear MPC in the microsecond range," *Automatica*, vol. 47, no. 10, pp. 2279–2285, 2011.

[21] S. Antonov, A. Fehn, and A. Kugi, "Unscented Kalman filter for vehicle state estimation," *Veh. Syst. Dyn.*, vol. 49, no. 9, pp. 1497–1520, 2011.

[22] L. Zhang, P. Guo, Z. Wang, and X. Ding, "An enabling tire-road friction estimation method for four-in-wheel-motor-drive electric vehicles," *IEEE Trans. Transp. Electrific.*, vol. 9, no. 3, pp. 3697–3710, 2023.

[23] S. Khaleghian, A. Emami, and S. Taheri, "A technical survey on tire-road friction estimation," *Friction*, vol. 5, no. 2, pp. 123–146, 2017.

[24] S. Roychowdhury, M. Zhao, A. Wallin, N. Ohlsson, and M. Jonasson, "Machine learning models for road surface and friction estimation using front-camera images," in *Proc. Int. Joint Conf. Neural Netw.*, 2018, pp. 1–8.

[25] V. Vassilev, "Road surface recognition at mm-wavelengths using a polarimetric radar," *IEEE Trans. Intell. Transp. Syst.*, vol. 23, no. 7, pp. 6985–6990, Jul. 2022.

[26] U. Montanaro et al., "Towards connected autonomous driving: Review of use-cases," *Veh. Syst. Dyn.*, vol. 57, no. 6, pp. 779–814, 2019.

[27] Volvo Car Group, "Volvo Cars puts 1000 test cars to use: Scandinavian cloud-based project for sharing road-condition information becomes a reality," Feb. 12, 2015. Accessed: Mar. 6, 2023. [Online]. Available: https://www.media.volvocars.com/uk/en-gb/media/pressreleases/157065/

[28] H. B. Pacejka, *Tire and Vehicle Dynamics*. Oxford, U.K.: Butterworth-Heinemann, 2012.

[29] Multi-Moby, "Multi-Moby—H2020 project," 2023. Accessed: Mar. 6, 2023. [Online]. Available: https://www.multi-moby.eu/

[30] V. Mazzilli et al., "On the benefit of smart tyre technology on vehicle state estimation," *Veh. Syst. Dyn.*, vol. 60, no. 11, pp. 3694–3719, 2022.

[31] H. Koylu and E. Tural, "Experimental study on braking and stability performance during low speed braking with ABS under critical road conditions," *Eng. Sci. Technol.*, vol. 24, no. 5, pp. 1224–1238, 2021.

[32] E. Giangiulio and D. Arosio, "New validated tire model to be used for ABS and VDC simulations," in *Proc. Tire Technol. Conf.*, 2006, pp. 1–5.

[33] R. D. McAllister and J. B. Rawlings, "Nonlinear stochastic model predictive control: Existence, measurability, and stochastic asymptotic stability," *IEEE Trans. Autom. Control*, vol. 68, no. 3, pp. 1524–1536, Mar. 2023.

[34] V. Ricciardi, D. Savitski, K. Augsburg, and V. Ivanov, "Estimation of brake friction coefficient for blending function of base braking control," *SAE Int. J. Passenger Cars-Mech. Syst.*, vol. 10, no. 3, pp. 774–785, 2017.

[35] "Regulation No 13-H of the Economic Commission for Europe of the United Nations (UN/ECE)—Uniform provisions concerning the approval of passenger cars with regard to braking [2015/2364]," *Official J. Eur. Union*, vol. 335, pp. 1–84, Dec. 2015.

[36] V. Wanaskar, S. Chaudhari, P. D. Shendge, and S. B. Phadke, "Extended nonlinear two-time scale estimation approach for antilock braking systems," *IEEE Trans. Ind. Electron.*, vol. 68, no. 10, pp. 10040–10049, Oct. 2021.

Gaetano Tavolo received the M.Sc. degree in mechanical engineering from the Politecnico di Torino, Turin, Italy, in 2020. He is currently working toward the Ph.D. degree in automotive engineering with the University of Surrey, Guildford, U.K.

His research interests include vehicle dynamics modeling and control applied to electric vehicles, with focus on advanced driver assistance systems.

Kai Man So received the B.Eng. and Ph.D. degrees in mechanical engineering from the National University of Singapore, Singapore, in 2012 and 2018, respectively.

He is currently a Research Fellow with the Centre for Automotive Engineering, University of Surrey, Guildford, U.K. His research interests include energy management and optimization of electric vehicles and vehicle dynamics control.

Davide Tavernini received the M.Sc. degree in mechanical engineering and the Ph.D. degree in dynamics and design of mechanical systems from the University of Padova, Padua, Italy, in 2010 and 2014, respectively.

He is currently a Senior Lecturer in advanced vehicle engineering with the University of Surrey, Guildford, U.K. His research interests include vehicle dynamics modeling and control, applied to over-actuated vehicles.

Pietro Perlo received the M.Sc. degree in general physics from the University of Torino, Turin, Italy, in 1980.

In 1981, he joined Centro Ricerche Fiat, Orbassano, Italy, where he was a Senior Director until 2011. Since 2011, he has been the President and owner of Interactive Fully Electrical VehicleS, Turin.

From 2013 to 2018, he was a member of the European Advisory Board on “Smart, Green and Integrated Transport”.

Aldo Sorniotti (Member, IEEE) received the M.Sc. degree in mechanical engineering and the Ph.D. degree in applied mechanics from the Politecnico di Torino, Turin, Italy, in 2001 and 2005, respectively.

He is currently a Full Professor in applied mechanics with the Politecnico di Torino, after being a Professor in advanced vehicle engineering with the University of Surrey, Guildford, U.K., where he led the Centre for Automotive Engineering. His research interest includes vehicle dynamics control for electric and automated vehicles.